Modeling the Interaction between the Atmospheric and Oceanic Boundary Layers, Including a Surface Wave Layer*

LE NGOC LY

Department of Agronomy, Iowa State University, Ames, IA 50011

(Manuscript received 26 August 1985, in final form 13 February 1986)

ABSTRACT

The interaction between the atmospheric and oceanic boundary layers is simulated by solving a closed system of equations including equations of motion, turbulent kinetic energy (TKE), turbulent exchange coefficient (TEC), expressions for air and sea stratification, and processes of air–sea interaction that account for the wave layer. The wave layer is characterized by discontinuities of velocity, TKE, and mean wind energy across the interface. The mechanism of energy transferred across the interface is taken into account by the method of bulk aerodynamic parameterization. Influences of wave effects on the vertical structure of air–sea turbulence and dynamics are studied numerically by variations of the surface wave state, and by variations of atmospheric stability.

The results demonstrate that diffusion plays an important part in the TKE budget, at least near the interface, and the wave layer acts as an additional source of TKE for the lower/upper parts of atmosphere/sea. The computational results show that waves influence both atmospheric and marine characteristics. This influence is especially large in the distributions of TKE on both sides of the interface, surface drift current velocity, wind velocity at the 10-m height, drag coefficient, and surface roughness. The results of the model are compared, where possible, with the observational data.

1. Introduction

The interaction between the atmosphere and ocean has long been recognized as an important process in the dynamic and thermodynamic behavior of both media. The transport of momentum and energy across the interface generates wind waves and drift currents which, in turn, affect subsequent vertical transport of momentum and energy.

Influences of surface waves on adjacent layers of the atmosphere and ocean have been noted by Roll (1965), Kitaigorodski and Miropolski (1969), Kitaigorodski (1970), Elder et al. (1970), Deleonibus (1971), Lai and Shemdim (1971), and Dubov et al. (1974). At present, there is not sufficient observational data to specify the quantitative influences of surface waves on the physical characteristics of the atmospheric and marine boundary layers.

The correct description of the wave layer is a major difficulty in the problems of air–sea interaction. The distinctive feature of the wave layer is that physical processes of this layer cannot be described by the Reynolds equations, and closure hypotheses for processes in this layer presently cannot be used. In my opinion, the wave layer should be taken into account in different problems of air–sea interaction because, through this wave layer, the exchanges of energy, momentum, heat, moisture, and salinity always occur. By studying the wave layer, we can better understand the mechanism of energy transfer from the atmosphere to the ocean through the separate mechanisms of the surface wave and the surface drift current. The influence of surface waves on the boundary layer structure of the ocean and atmosphere, although there have been numerous experimental investigations and analytical studies, is still poorly understood.

It is generally recognized that TKE production is connected only to the interaction between Reynolds stress and the field of mean velocity (see Laikhtman, 1966, 1970; Yeh, 1973, 1974; Mellor and Durbin, 1975). However, in another model (Kitaigorodski, 1970), it was suggested that the main mechanism for TKE production in the marine surface layer is the diffusive flux of TKE from the air–sea transitional layer where the energy of surface wave breaking is transformed into marine TKE. He further suggested that the shearing of velocity vector plays a small role in comparison with diffusion of TKE. Therefore, it is likely that the TKE production is related both to the shearing of the mean velocity vector and to the diffusive flux of TKE. The problem then is what mechanism for TKE production predominates in specific situations.

Kalatski (1969) solved a three-layer problem in which the wind wave layer was considered as a fictitious fluid with density having a prescribed distribution. Obviously, such an idealized three-layer problem was too

* Journal Paper J-11984 of the Iowa Agriculture and Home Economics Experiment Station, Ames, IA, Project 2521.

simple to characterize the air–sea interaction (ASI) problem if the wave layer is taken into account. The traditional approach in treating the wave layer in boundary layer modeling is that it is forced to collapse into the form of a flat interface across which there is no discontinuity of physical characteristics between the atmosphere and sea. In this traditional approach of describing the wave layer, its influences are expressed by means of the roughness effect of an oscillating marine surface, which is represented by the roughness length z_0. Here, one assumes continuous conditions of various physical characteristics across the air–sea interface (Laikhtman, 1966, 1970; Yeh, 1973, 1974; Tarnopolski and Shnaydman, 1984).

In some recent studies, Klein and Coantic (1981) used the TKE flux from the atmosphere associated with the wave effect as a boundary condition in their thermocline marine mixed-layer model, and Egorov (1984) used the TKE flux from the wave surface in his model to study the wave influence on air flow over water. By using traditional boundary conditions, Tarnopolski and Shnaydman (1984) solved the air–sea interaction problem, taking into account the wave effect by modifying the von Karman formula for the marine mixing length (l_2) by making it proportional to the wind wave height. In summary, the wave layer should not be considered a plane surface having no discontinuity, because discontinuities of different physical characteristics are expected to exist across the air–water interface.

In this paper, I investigate coupled boundary layer problems by taking into account the wave layer. The mechanism of energy transfer across the air–sea interface is taken into account by a method of bulk parameterization. The influences of the surface wave and variations of atmospheric stratification on turbulent structure and dynamics in the boundary layers of the atmosphere and sea are studied by numerical experiments.

2. The governing equations and boundary conditions

The present study assumes that stationary and horizontally homogeneous conditions exist. Governing equations for the model (Yeh, 1974) include equations of motion, TKE, TEC, and expressions for atmospheric and sea stratification. Such a system of equations can be written in the same form for both atmospheric and sea boundary layers (ASBL). The subscript $i = 1$ represents variables in the atmosphere and $i = 2$ represents those in the water body.

a. The equations of motion and turbulent kinetic energy

We incorporate the equations of motion in Cartesian form (see Yeh, 1973, 1974)

$$\frac{d}{dz_i}K_i\frac{du_i}{dz_i} + fv_i = \frac{1}{\rho_i}\frac{\partial P_i}{\partial x_i}; \quad \frac{d}{dz_i}K_i\frac{dv_i}{dz_i} - fu_i = \frac{1}{\rho_i}\frac{\partial P_i}{\partial y_i} \tag{1}$$

where x_i, y_i, z_i are coordinates such that the x_i-axes are in the direction of surface stress vector, z_i-axes are in the direction, up for atmosphere and down for sea; u_i and v_i are components of wind and seawater drift current velocities; K_i are the vertical TEC for the atmosphere and sea; f is the Coriolis parameter ($f = 2\omega \times \sin\phi$; ω is angular velocity of the earth's rotation and ϕ is latitude); ρ_i are the densities of air and seawater; P_i are pressures, which are written in terms of the geostrophic wind (U_{g1}) and the geostrophic current (U_{g2}).

The turbulent exchange coefficient can be expressed in terms of TKE (Blackadar, 1962; Laikhtman, 1979) as

$$K_i = l_i E_i^{1/2} = -kc^{1/4}\frac{E_i/K_i}{\dfrac{d}{dz_i}(E_i/K_i)}E_i^{1/2}$$

$$= kE_i\left(\frac{K_{0i}}{E_{0i}} + \int_{z_{0i}}^{z_i}\frac{dz_i}{E_i^{1/2}}\right) \tag{2}$$

where k is the von Karman constant assumed here to be 0.40, z_{0i} are the roughness lengths of air–sea interface, K_{0i} and E_{0i} are TEC and TKE at z_{0i}, and l_i are the mixing lengths determined for thermally stratified flow using the von Karman similarity hypothesis (Zilitinkevich and Laikhtman, 1965).

The equation for TKE is written in the following form for thermally stratified turbulent flow (Monin and Yaglom, 1965; Takle et al., 1982).

$$K_i\left[\left(\frac{du_i}{dz_i}\right)^2 + \left(\frac{dv_i}{dz_i}\right)^2 - \frac{g}{\theta_i^0}\frac{d\theta_i}{dz_i}\right] + \alpha_e\frac{d}{dz_i}K_i\frac{dE_i}{dz_i} = c\frac{E_i^2}{K_i} \tag{3}$$

where g is acceleration of gravity, θ_i represents the potential temperature in the atmosphere ($\theta_i = \theta_1$) and for the sea, $\theta_i = \rho_2$ (ρ is density); θ_i^0 are the average air temperature (θ_1^0) and the seawater density (ρ_2^0) in the boundary layers; E_i represents the TKE; $\alpha_e = (K_e/K_i)$ and c are assumed to be dimensionless constants; $\alpha_e = 0.73$, $c = 0.046$; K_e is the TEC for vertical diffusion of TKE (see Monin and Yaglom, 1965).

The momentum fluxes are denoted as

$$\eta_i = K_i\frac{du_i}{dz_i}; \quad \sigma_i = K_i\frac{dv_i}{dz_i} \tag{4}$$

where η_i and σ_i represent the X and Y components, respectively.

Equations (1) and (3) may be written in the form

$$\frac{d^2\eta_i}{dz_i^2} + f\frac{\sigma_i}{K_i} = 0; \quad \frac{d^2\sigma_i}{dz_i^2} - f\frac{\eta_i}{K_i} = 0 \tag{5}$$

$$\frac{\eta_i^2 + \sigma_i^2}{K_i} - K_i\frac{g}{\theta_i^0}\frac{d\theta_i}{dz_i} - c\frac{E_i^2}{K_i} + \alpha_e\frac{d}{dz_i}K_i\frac{dE_i}{dz_i} = 0. \tag{6}$$

b. The density gradients

To simplify modeling the air–sea interaction, the approximate formulas for the vertical gradients of air temperature and seawater density have been employed to close the system (1)–(3). The vertical gradient of air temperature is determined by the interpolation formula (Laikhtman, 1961, 1970)

$$\frac{d\theta_1}{dz_1} = -\frac{Q_0}{\rho_1 c_p k u_{*1} z_1} + (\gamma_a - \gamma_p) \tag{7}$$

where c_p is the specific heat for air at constant pressure; u_{*1} is the friction velocity of the atmosphere, γ_a is the dry adiabatic lapse rate, γ_p is the actual lapse rate at the upper part of the atmospheric boundary layer, Q_0 is the vertical heat flux at the interface.

The vertical distribution of seawater density is approximated by the following formulas (Ly, 1981)

$$\frac{d\rho_2}{dz_2} = \tilde{A}\rho_2\delta(z_2 - z_c) + (\Gamma_1 - \Gamma_2)\sigma(z_2 - z_c) + \Gamma_2 \tag{8}$$

where

$$\delta(z_2 - z_c) = \begin{cases} 0, & \text{if } z_2 \neq z_c \\ \infty, & \text{if } z_2 = z_c \end{cases}$$

$$\sigma(z_2 - z_c) = \begin{cases} 0, & \text{if } 0 \leqslant z_2 < z_c \\ 1, & \text{if } z_2 \geqslant z_c. \end{cases}$$

Here $\tilde{A}$ is a characteristic parameter for the magnitude of a jump in seawater density layer, z_c is the depth of the seawater density-jump layer, $\delta(z_2 - z_c)$ is the delta function, $\sigma(z_2 - z_c)$ is the unit function, and Γ_1 and Γ_2 are the vertical gradients of seawater density in the water layers lying below and above the density-jump layer.

c. The wave layer

Because the thickness of the wave layer is small (of order of the magnitude of the wave height) in comparison with heights of air and sea boundary layers, we assume in the steady-state condition that the shear stress or the momentum transfer and the Y-component of velocity are continuous across the interface

$$K_1\rho_1 \left.\frac{du_1}{dz_1}\right|_{z_1=z_{01}} = -K_2\rho_2 \left.\frac{du_2}{dz_2}\right|_{z_2=z_{02}};$$

$$K_1\rho_1 \left.\frac{dv_1}{dz_1}\right|_{z_1=z_{01}} = -K_2\rho_2 \left.\frac{dv_2}{dz_2}\right|_{z_2=z_{02}} \tag{9}$$

$$v_1(z_1)|_{z_{01}} = v_2(z_2)|_{z_{02}} \tag{10}$$

where z_{01} and z_{02} are the roughness lengths of the upper and the lower bounds of interface.

If a wave layer is to persist in a steady-state situation, it must continually be supplied with energy from the mean and TKE fields of the adjacent fluids. The hydrodynamic characteristics of the wave layer may be assumed to be functions of air friction velocity (u_{*1}), acceleration of gravity (g), air density (ρ_1) and seawater density (ρ_2). Based on conservation of energy and dimensional analysis, we have the following formula for the TKE flux (see Fig. 1):

$$K_1\rho_1 \left.\frac{dE_1}{dz_1}\right|_{z_{01}} + K_2\rho_2 \left.\frac{dE_2}{dz_2}\right|_{z_{02}} = C_1\rho_1 u_{*1}^3 \tag{11}$$

where C_1 is understood as a dimensionless parameter representing the surface wave layer. Similar reasoning leads to an equation for mean wind energy flux transferred to water:

$$K_1\rho_1 \left.\frac{du_1}{dz_1}u_1\right|_{z_{01}} + K_2\rho_2 \left.\frac{du_2}{dz_2}u_2\right|_{z_{02}} = C_1\rho_1 u_{*1}^3 \tag{12}$$

where C_1 describes the size of the wave layer and intensity of the wind surface wave, and each value of C_1 is matched to a marine surface state in the interface. By variation of parameter C_1, we can numerically study influences of the effects of waves on the structure of air–sea boundary layers. It should be noted that $C_1 = 0$ gives the traditional conditions of continuity for air–water characteristics across the interface.

The bottom boundary condition on TKE for the atmosphere is conventionally given as $E_1 = \alpha u_{*1}^2$ (Wyngaard, 1975), so at the upper (z_{01}) and the lower (z_{02}) bounds of the wave layer, I suggest the hypothesis for TKE that the ratio of TKE at the interface be equal to the ratio of the square of the friction velocities:

$$\left.\frac{E_1(z_1)}{E_2(z_2)}\right|_{z_{01},z_{02}} = \left(\frac{u_{*1}}{u_{*2}}\right)^2. \tag{13}$$

From this equation and the assumption that the roughness lengths are functions of u_{*1}, g, ρ_1 and ρ_2, one can get Charnock's formula (Charnock, 1955) for both bounds of the interface by the method of dimensional analysis:

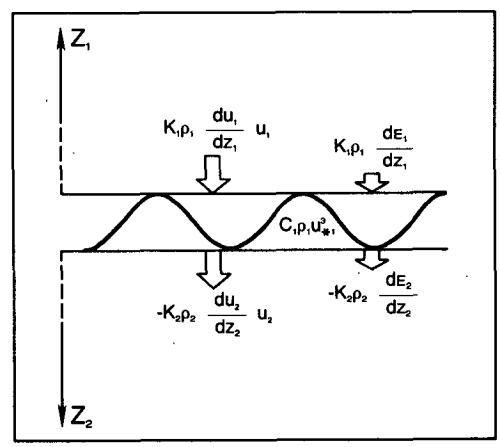

FIG. 1. Energy transfer across the air–sea interface.

$$z_{0i} = \frac{u_{*i}^2}{g} a\left(\frac{\rho_1}{\rho_2}\right) \tag{14}$$

where the function $a(\rho_1/\rho_2)$ may be taken as an empirical constant equal to 0.05 (e.g., Roll, 1965; Kitaigoroddski, 1970). Equations (9)–(13) become boundary conditions at the interface of the air–sea boundary layers. The top boundary conditions are such that the velocities tend to constants and the momentum flux and TKE are zero:

$$u_i(z_i)|_{z_{Hi}} \to u_{gi}; \quad v_i(z_i)|_{z_{Hi}} \to v_{gi} \tag{15}$$

$$K_i \frac{du_i}{dz_i}\bigg|_{z_{Hi}} \to 0; \quad K_i \frac{dv_i}{dz_i}\bigg|_{z_{Hi}} \to 0; \quad E_i(z_i)|_{z_{Hi}} \to 0. \tag{16}$$

Boundary conditions (9) and (16) required for the solution of (5) and (6) can be written as

$$\eta_i(z_i)|_{z_{0i}} \to u_{*i}^2; \quad \sigma_i(z_i)|_{z_{0i}} \to 0 \tag{17}$$

$$\eta_i(z_i)|_{z_{Hi}} = \sigma_i(z_i)|_{z_{Hi}} \to 0; \quad E_i(z_i)|_{z_{Hi}} \to 0. \tag{18}$$

Equations (2) and (4)–(8) with boundary conditions (9)–(14) and (17), (18) allow simulation of the air–sea coupled boundary layers, taking into account the wave layer and fluxes across the interface.

3. The set of equations in dimensionless form

For convenience, the problem is solved in dimensionless form. The dimensionless quantities are adopted as follows:

$$u_i^n = (-1)^{i+1}(k/u_{*i})u_i; \quad v_i^n = (-1)^{i+1}(k/u_{*i})v_i;$$
$$z_i^n = fz_i/(ku_{*i}) = z_i/\lambda_i; \quad E_i^n = c^{1/2}E_i/u_{*i}^2;$$
$$K_i^n = K_i/(ku_{*i}\lambda_i); \quad \eta_i^n = (-1)^{i+1}\eta_i/u_{*i}^2;$$
$$\sigma_i^n = (-1)^{i+1}\sigma_i/u_{*i}^2 \tag{19}$$

where $\lambda_i = ku_{*i}/f$ is about the order of the planetary boundary layer thickness, c is an empirical dimensionless constant (assumed equal to 0.046).

The system of equations with the transformations given by (19) is written in the dimensionless form (the superscript n hereafter signifies any quantity in the dimensionless form) as follows:

$$\frac{d^2\eta_i^n}{(dz_i^n)^2} + \frac{\sigma_i^n}{K_i^n} = 0; \quad \frac{d^2\sigma_i^n}{(dz_i^n)^2} - \frac{\eta_i^n}{K_i^n} = 0 \tag{20}$$

$$\frac{(\eta_i^n)^2 + (\sigma_i^n)^2}{K_i^n} - K_i^n R_i - \frac{(E_i^n)^2}{K_i^n} + \beta \frac{d}{dz_i^n} K_i^n \frac{dE_i^n}{dz_i^n} = 0 \tag{21}$$

$$K_i^n = l_i^n (E_i^n)^{1/2} = -\frac{(E_i^n)^{3/2}/K_i^n}{\dfrac{d}{dz_i^n}(E_i^n/K_i^n)}$$

$$= E_i^n\left[\frac{K_{0i}^n}{E_{0i}^n} + \int_{z_{0i}^n}^{z_i^n} \frac{dz_i^n}{(E_i^n)^{1/2}}\right] \tag{22}$$

where K_{0i}^n and E_{0i}^n are the dimensionless TEC and dimensionless TKE, respectively, at a roughness height, respectively (Ly, 1984).

$$\left.\begin{aligned} R_i &= (R_1, R_2) \\ R_1 &= (\mu/z_i^n) + \nu_0 \end{aligned}\right\} \tag{23}$$

$$R_2 = \frac{k^4}{f^2}\frac{g}{\rho_2^0} \times \left(\frac{\Delta\rho_2}{\pi}\frac{m}{1+b^2} + \frac{\Gamma_1 - \Gamma_2}{\pi}\tan^{-1}b + \frac{\Gamma_1 - \Gamma_2}{2}\right) \tag{24}$$

where $b = m(z_2^n - z_c^n)$; R_1 and R_2 describe the thermal and density stratifications in boundary layers.

$$\mu = -\frac{g}{\theta_1^0}\frac{k^2 Q_0}{\rho_1 c_p f u_{*1}^2} = \lambda_1/L_1 \tag{25}$$

where μ is a parameter for atmospheric thermal stratification (Kazanski and Monin, 1960), Q_0 is the vertical turbulent heat flux at the interface; and μ is the ratio of the length scale for the atmospheric boundary layer $\lambda_1 = (ku_{*1})/f$ and the length scale for the atmospheric surface layer (Monin–Obukhov length scale) $L_1 = -u_{*1}^3/[k(g/\theta_1^0)(Q_0/\rho_1 c_p)]$ (Monin and Obukhov, 1954).

$$\nu_0 = gk^4(\gamma_a - \gamma_p)/(\theta_1^0 f^2) \tag{26}$$

where ν_0 is a parameter for atmospheric stratification at the upper part of the boundary layer (Laikhtman, 1970); $\Delta\rho_2$ is the drop of seawater density in the density-jump layer; m is a parameter controlling the shape of seawater density distribution; and β is a constant ($\beta = 0.54$) (Monin and Yaglom, 1965).

The boundary conditions in the dimensionless form are for $z_i^n \to z_{0i}^n$

$$\eta_1^n(z_1^n)|_{z_{01}^n} = \eta_2^n(z_2^n)|_{z_{02}^n} = 1$$
$$\sigma_1^n(z_1^n)|_{z_{01}^n} = \sigma_2^n(z_2)|_{z_{02}^n} = 0. \tag{27}$$

From (11) and (13) we have conditions (28) and (29) for TKE, E_i^n:

$$\left[K_1^n \frac{dE_1^n}{dz_1^n} + \left(\frac{\rho_1}{\rho_2}\right)^{1/2} K_2^n \frac{dE_2^n}{dz_2^n}\right]\bigg|_{z_{0i}^n} = \frac{c^{1/2}C_1}{k} \tag{28}$$

$$E_1^n(z_1^n)|_{z_{01}^n} = E_2^n(z_2^n)|_{z_{02}^n}. \tag{29}$$

From (9) and (10), we have

$$\rho_1 u_{*1}^2|_{z_{01}^n} = \rho_2 u_{*2}^2|_{z_{02}^n} \tag{30}$$

$$v_1^n|_{z_{01}^n} = -\left(\frac{\rho_1}{\rho_2}\right)^{1/2} v_2^n\bigg|_{z_{02}^n} \tag{31}$$

and from (12), we have a discontinuous condition for the X-component of velocity

$$u_1^n|_{z_{01}^n} = -\left(\frac{\rho_1}{\rho_2}\right)^{1/2} u_2^n|_{z_{02}^n} + C_1 k. \tag{32}$$

For $z_i^n \to z_{Hi}^n$, we have

$$[\eta_i^n(z_i^n), \sigma_i^n(z_i^n)]|_{z_{Hi}^n} = 0 \tag{33}$$

$$E_i^n(z_i^n)|_{z_{Hi}^n} = 0. \tag{34}$$

4. Method of solution

The following formulas for dimensionless wind and drift current profiles can be obtained by substituting (19) into (1). The wind profiles in the atmosphere are as follows:

$$u_1^n = \frac{k}{u_{*1}} U_{g1} \cos\alpha_1 + \frac{d\sigma_1^n}{dz_1^n}$$

$$v_1^n = \frac{k}{u_{*1}} U_{g1} \sin\alpha_1 - \frac{d\eta_1^n}{dz_1^n}. \tag{35}$$

The drift current profiles in the sea are

$$u_2^n = \frac{k}{u_{*2}} U_{g2} \cos\alpha_2 + \frac{d\sigma_2^n}{dz_2^n}$$

$$v_2^n = -\frac{k}{u_{*2}} U_{g2} \sin\alpha_2 - \frac{d\eta_2^n}{dz_2^n} \tag{36}$$

where

$$U_{gi} \cos\alpha_i = -\frac{1}{f\rho_i}\frac{\partial P_i}{\partial y_i}; \quad U_{gi} \sin\alpha_i = \frac{1}{f\rho_i}\frac{\partial P_i}{\partial x_i}$$

are the geostrophic velocity components and α_i are the angles between the surface stress and geostrophic wind ($i = 1$) and geostrophic current ($i = 2$).

Substituting (35) and (36) into (31) and (32), we have the following formulas linking atmospheric and oceanic boundary layers:

$$\left.\begin{aligned} &\frac{k}{u_{*1}} U_{g1} \cos\alpha_1 + \left.\frac{d\sigma_1^n}{dz_1^n}\right|_{z_{01}^n} \\ &\quad = \left(\frac{\rho_1}{\rho_2}\right)^{1/2}\left(\frac{k}{u_{*2}} U_{g2} \cos\alpha_2 - \left.\frac{d\sigma_2^n}{dz_2^n}\right|_{z_{02}^n}\right) + kC_1 \\ &\frac{k}{u_{*1}} U_{g1} \sin\alpha_1 - \left.\frac{d\eta_1^n}{dz_1^n}\right|_{z_{01}^n} \\ &\quad = \left(\frac{\rho_1}{\rho_2}\right)^{1/2}\left(\frac{k}{u_{*2}} U_{g2} \sin\alpha_2 + \left.\frac{d\eta_2^n}{dz_2^n}\right|_{z_{02}^n}\right) \end{aligned}\right\}. \tag{37}$$

Having (37), we can easily obtain the geostrophic coefficient (χ) and angle (α_1).

$$\chi^2 = \left(\frac{u_{*1}}{kU_{g1}}\right)^2 = \frac{[1 - 2n\cos\beta_1 + n^2 + A + (kC_1\chi)^2]}{M_1^2 + M_2^2} \tag{38}$$

$$\tan\alpha_1 = -\frac{M_1 - n(M_2 \sin\beta_1 + M_1 \cos\beta_1) - (M_1\chi kC_1)/\cos\alpha_1}{M_2 - n(M_1 \cos\beta_1 - M_2 \sin\beta_1)} \tag{39}$$

where $n = U_{g2}/U_{g1}$; $\beta_1 - 360° = \alpha_2 - \alpha_1$; $(\rho_1/\rho_2)^{1/2} \approx 1/28$; β_1 is the angle between the geostrophic wind and geostrophic current (e.g., Laikhtman, 1970).

$$A = 2kC_1\chi(n\cos\alpha_2 - \cos\alpha_1)$$

$$M_1 = \left.\left(\frac{d\eta_1^n}{dz_1^n} + \frac{1}{28}\frac{d\eta_2^n}{dz_2^n}\right)\right|_{z_{0i}^n}$$

$$M_2 = \left.\left(\frac{d\sigma_1^n}{dz_1^n} - \frac{1}{28}\frac{d\sigma_2^n}{dz_2^n}\right)\right|_{z_{0i}^n}.$$

From (14) and (19), we have the formulas for dimensionless roughness lengths

$$z_{01}^n = (afU_{g1}\chi)/g \tag{40}$$

$$z_{02}^n = 28(afU_{g1}\chi)/g \tag{41}$$

where a is the Charnock empirical constant. The drag coefficient C_D is found as

$$C_D = \left(\frac{u_{*1}}{U_{10}}\right)^2 = (kU_{g1}\chi/U_{10})^2. \tag{42}$$

Profiles of TEC are calculated by the formulas

$$K_1(z_1) = \frac{k^4U_{g1}^2}{f}\chi^2K_1^n(z_1^n) \tag{43}$$

$$K_2(z_2) = \left(\frac{1}{28}\right)^2\frac{k^4U_{g1}^2}{f}\chi^2K_2^n(z_2^n). \tag{44}$$

It can be noted that the parameter C_1 representing the wave layer is present in (38) and (39) and, through these terms, affects other characteristics of the atmospheric and marine boundary layers. Equation (12) shows the physical link between C_1, wind speed and wave growth. This shows that a larger C_1 means that more energy is transferred from the wind to the surface wave ($C_1\rho_1u_{*1}^3$).

Equations (20)–(34) are solved numerically by a finite difference method and iteration to find $K_i^n(z_i^n)$ and $E_i^n(z_i^n)$. In the first iteration, $K_i^n(z_i^n) = z_i^n$ for TEC and $E_i^n(z_i^n) = 1$ for TKE. The grid used for the simulations consisted of 100 irregularly spaced points. The domain of integration ranges from $z_i^n = 0$ to 1 for each boundary layer. The value of $E_i^n(z_i^n) = 1$ is obtained from (21) by setting the diffusive flux to zero at z_{0i} (Zilitinkevich, 1970). The solution to the problem proceeds in the following order. First, the simulation process for atmosphere is done by solving Eq. (20) with conditions (27) and the approximation for TEC, $K_i^n(z_i^n) = z_i^n$. Equation (21) for the atmosphere is then solved with the "new" η_i^n, σ_i^n and the approximate value, $E_i^n(z_i^n) = 1$. Then K_i^n is computed from Eq. (22). By using the "new" value of E_1^n for the atmosphere, the value of E_2^n at z_{02}^n for the sea may be found by Eq. (28). The same procedure is repeated for the sea. The entire iteration procedure is completed when Eq. (29) is satisfied.

After having distributions of dimensionless functions η_i^n, σ_i^n, K_i^n, E_i^n, $(d\eta_i^n/dz_i^n)$ and $(d\sigma_i^n/dz_i^n)$, one can calculate the distributions of dimensionless wind velocity, drift current velocity, the geostrophic coefficient χ, angle α_1, and air–sea interaction characteristics of both boundary layers by formulas (35)–(44). By using (19), one can easily recover dimensional characteristics from dimensionless ones.

Equations (20)–(34) may be solved with much less computing time and a simpler procedure. Near the wave layer, the effect of buoyancy may be ignored. Then, (2) may be written in the form

$$\alpha_e \frac{d}{dz_i} K_i \frac{dE_i}{dz_i} - c\frac{E_i^2}{K_i} + \frac{u_{*i}^4}{K_i} = 0. \tag{45}$$

From Eq. (13), the following conditions for TKE must be satisfied at the boundaries of the wave layer

$$E_i(z_i)|_{z_{0i}} = \gamma u_{*i}^2 \tag{46}$$

where γ is a dimensionless parameter to be determined. After some transformations with notation $(dz_i/K_i) = d\xi_i$, and by using (46) for the nonlinear term, $(E_i)^2$, (45) may be written in the form

$$\frac{d^2E_i}{d\xi_i^2} - \frac{c\gamma u_{*i}^2}{\alpha_e} E_i + \frac{u_{*i}^4}{\alpha_e} = 0. \tag{47}$$

Equation (47) with the boundary condition for E_i in (18) has the following analytical solution

$$E_i(\xi_i) = u_{*i}^2\left\{\left(\gamma - \frac{1}{c\gamma}\right)\exp\left[-\left(\frac{c}{\alpha_e}\right)^{1/2} u_{*i}\xi_i\right] + \frac{1}{c\gamma}\right\}. \tag{48}$$

With (48), (11) may be written as

$$\left(\frac{c\gamma}{\alpha_e}\right)^{1/2}\left(\gamma - \frac{1}{c\gamma}\right)\left[u_{*1}^3 + \left(\frac{\rho_2}{\rho_1}\right)u_{*2}^3\right] = -C_1 u_{*1}^3. \tag{49}$$

Substitution of (30) into (49) gives the equation for calculating values of γ from the values of the parameter C_1:

$$\left(\frac{c\gamma}{\alpha_e}\right)^{1/2}\left(\frac{1}{c\gamma} - \gamma\right)\left[1 + \left(\frac{\rho_1}{\rho_2}\right)^{1/2}\right] = C_1 \tag{50}$$

where γ is a dimensionless parameter and c is assumed here to be a dimensionless constant ($c = 0.046$) (e.g., Monin and Yaglom, 1965). If $C_1 = 0$ in Eq. (50), γ is equal to $c^{-1/2}$ and (46) becomes $E_i(z_i)|_{z_{0i}} = c^{-1/2}u_{*1}^2$, which is a traditional boundary condition for TKE in ASI problems (see Laikhtman, 1970; Zilitinkevich, 1970). By using (46) and (50), with the boundary conditions (27) and (30)–(34), Eqs. (20)–(26) may be solved separately for the atmosphere and sea.

5. Model initial inputs and outputs

a. Initial inputs of the model

The initial inputs of the model are the "external parameters" of atmospheric and oceanic BL. These external parameters are geostrophic wind (U_{g1}), geostrophic current (U_{g2}), or equivalently the ratio $n = U_{g2}/U_{g1}$, and the angle β_1 between U_{g1} and U_{g2}. The values of those parameters were taken to be, $U_{g1} = 5$, 10, 15 and 20 m s^{-1}; $n = 0.02$; and $\beta_1 = \pi/4$ and latitude $\phi = 45°$.

To simplify the modeling process and to focus attention on the study of the wave layer, the typical values of stratification of the atmosphere μ in formula (25) were considered to range from -100 to 100 (see Yeh, 1973) and also typical seawater density gradients $\Gamma_1 = 10^{-3}$ kg m^{-4}; $\Gamma_2 = 6.10^{-3}$ kg m^{-4} and the drop of density $\Delta\rho_2 = 1.7$ kg m^{-3}. All the above external parameters of the model could be calculated based on the standard hydrometeorological observational data (see Zilitinkevich, 1970; Tarnopolski and Shnaydman, 1984). Based on analysis of the order of magnitude of the surface wind and current speeds in Eq. (12), C_1 was allowed to have values 0 (the wave layer is not taken into account as in all air–sea interaction models to date), 1 and 10 in the simulations. Larger values of C_1 correspond to larger wave layers; i.e., the surface wave becomes higher.

b. The model outputs

The outputs of the model are profiles of different characteristics describing the dynamic and turbulent structure of the boundary layers of the atmosphere and the adjacent sea and also different characteristics of the interaction. They include profiles of shear stress, TEC, TKE, components of the TKE budget, wind speed and wind drift current for both atmospheric and oceanic boundary layers at different stratification of atmosphere, geostrophic wind, and parameter C_1.

The outputs of the model also include characteristics of the interaction such as wind velocity at the 10-m height (U_{10}), surface drift current velocity (U_{02}), roughness parameter (z_0), friction velocity (u_{*1}), geostrophic wind coefficient (C_A), drag coefficient (C_D), angles (α_1), geostrophic coefficient (χ), heights of atmospheric and oceanic BL(H_i), and TEC of both BL at 1% of BL height at different atmospheric stability. In this paper, we present only a few of the outputs of the model.

6. Results and comparisons

The numerical results of the model are presented in Table 1 and Figs. 2–19. The basic ASI characteristics are shown in Table 1. The table shows that the wave layer influences almost all basic ASI characteristics. This influence increases with increasing U_{g1} and C_1. The results in the table for $U_{g1} = 15$ m s^{-1} and $C_1 = 1$ are in good agreement with observational data from the weather ship on 15 February 1981 at the oceanic station C (52.7°N, 35.5°W) (see Tarnopolski and Shnaydman, 1984), which are as follows: $U_{g1} = 14$ m s^{-1}, $U_{10} = 10.3$ m s^{-1}, $u_{*1} = 0.35$ m s^{-1}, $C_D = 1.17$;

TABLE 1. Basic characteristics of air-sea interaction for the neutral condition of atmosphere. The first number given is for $C_1 = 1$, and the second is for $C_1 = 0$.

U_{g1} (m s^{-1})	$10^5 z_0$ (m)	U_{10} (m s^{-1})	$10^2 U_{02}$ (m s^{-1})	u_{*1} (m s^{-1})	$10^2 C_A$	$10^3 C_D$	$-\alpha_1$ (deg)	$10^{-3}\chi$
5	8.13	3.89	12.92	0.13	2.58	1.05	14.2	63
	8.57	3.84	13.27	0.13	2.65	1.14	15.3	65
10	35.4	7.18	25.40	0.26	2.54	1.35	14.9	66
	37.4	7.10	26.10	0.27	2.61	1.47	16.0	68
15	84.5	10.10	37.70	0.41	2.51	1.62	15.3	68
	89.3	9.90	39.00	0.42	2.58	1.78	16.5	70
20	160.0	12.90	50.00	0.56	2.54	1.78	15.8	70
	169.0	12.30	52.20	0.58	2.61	2.19	17.1	72

$-\alpha_1 = 15.3$ (deg), $\chi = 0.066$ and wave height $h = 2.5$ m.

Figures 2 and 3 show the vertical distributions of dimensionless shear stress in both boundary layers (BL). The dimensionless functions of shear stress are near zero at $Z_i^n \rightarrow Z_{Hi}^n$. Atmospheric stratification noticeably influences the shear stress in the atmosphere but has almost no influence on the shear stress in the sea. The vertical profiles of Y-components of shear stress, σ_1^n and σ_2^n, show that all values increase nearly linearly for some distance from the surface and then drop sharply to zero. From these figures, we can see that the greater the instability, the higher is the maximum point that can be reached. That means the BL height increases with growing instability in the atmosphere. It is noted that the wave effects have practically no influence on η_i^n and σ_i^n. The model results of shear stress agree qualitatively with those obtained by Deardorff (1972) and Yeh (1973).

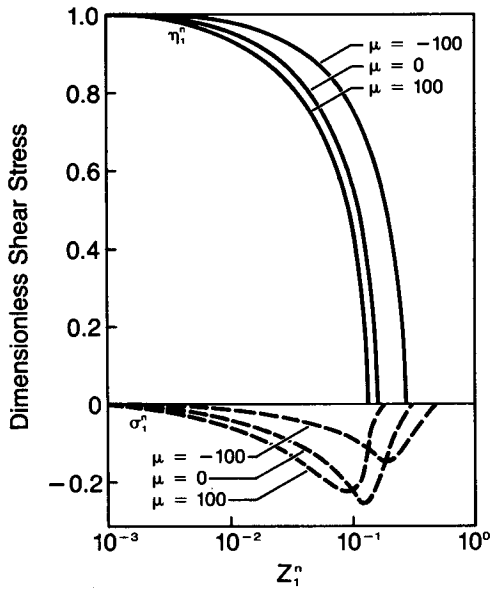

FIG. 2. Vertical profiles of the components of dimensionless shear stress (η_1^n and σ_1^n) in ABL for the different atmospheric stratification (μ).

Figures 4 and 5 show the distributions of dimensionless TKE in the ASBL with different μ and C_1. From these figures, we can see that the values of E_1^n and E_2^n increase with instability. Obviously, μ strongly influences the distribution of TKE in the upper part of the atmospheric BL (ABL) and has much less effect on TKE of the sea BL (SBL). For the small values of z_i^n, TKE is independent of atmospheric stability [i.e., $(\partial E_i^n/\partial\mu) = 0$] and has almost the same values for the sea. For $C_1 = 0$, and an unstable ABL condition ($\mu < 0$), E_1^n first increases with height (because of thermal effects), then reaches a maximum at a certain height (higher values for higher instability), and finally decreases to zero at the upper bounds of BL. For the stable condition ($\mu > 0$), there is a smooth diminishing of TKE with height. In the SBL, TKE decreases with depth for all conditions of μ and has only weak dependence on μ.

Figures 4 and 5 also show the TKE distributions at different C_1. From these profiles, it is very clear how the wave layer influences distributions of TKE in the atmosphere and sea. Here, we see that the influence of the wave layer on TKE in the lower/upper parts of the atmosphere/sea is practically independent of μ. On the

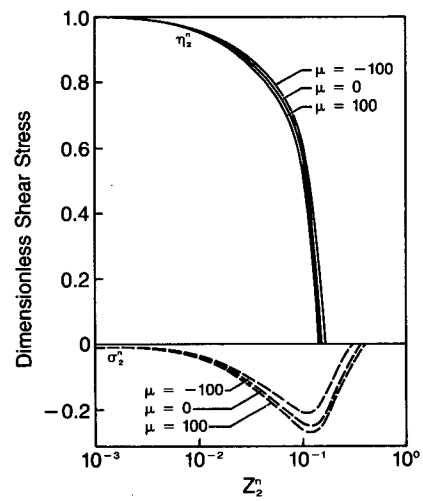

FIG. 3. As in Fig. 2 but for η_2^n and σ_2^n in SBL.

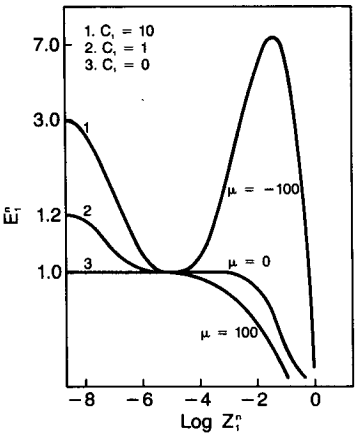

FIG. 4. Vertical profile of the dimensionless TKE in ABL at different μ and wave effect parameter, C_1.

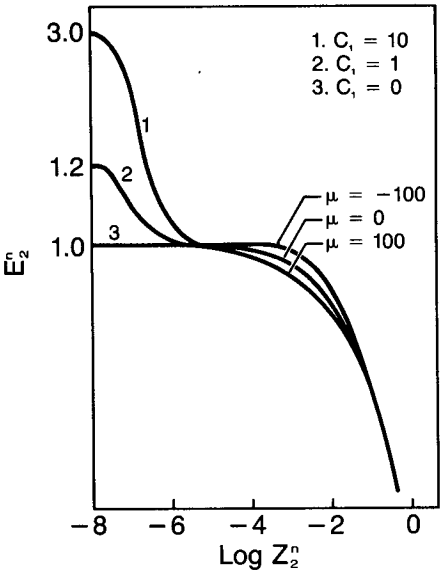

FIG. 5. As in Fig. 4 but in the sea.

other hand, for the zone of large values of z_i^n, TKE is independent of the wave effect; i.e., $(\partial E_i^n/\partial C_1) = 0$. It is clear from these graphs that E_1^n and E_2^n rather rapidly decrease to the "nonstirred-up levels." Far from the wave layer, the air and water turbulent flows are essentially the same as air flow over land and water flow with no waves, and interaction between the waves and the turbulent flow practically may be neglected. From the graphs in Figs. 4 and 5, we can interpret the wave layer as an additional source of turbulence in the lower/upper parts of atmosphere/sea. It is worth noting that the variation of the wave effect can be adjusted by the variations of parameter C_1 in the model.

There are no observational data of TKE in the atmosphere and sea to compare with these model results. We found only some indirect estimates and calculations from other models. Based on observational data (weather ship on 15 February 1981), Tarnopolski and Shnaydman (1984) calculated TKE for SBL and obtained $E_2(z_{02}) = 6.10^{-4}$ m^2 s^{-2} at roughness length z_{02} with the wave height $h = 2.5$ m and $E_2(z_{02}) = 8.10^{-4}$ m^2 s^{-2} with $h = 3.5$ m. These values match the dimensionless values of $E_2^n \approx 3$ and $E_2^n \approx 4$. Investigating the wave influence on the dynamic structure of the flow over water, Egorov (1984) used the estimate of the TKE flux from the WL to the atmosphere given by Dubov et al. (1974) to calculate the dimensionless TKE at z_{01}^n and got $E_1^n(z_{01}^n) = 3.3$ for the case of the developing wave. The present model results of TKE at z_{0i}^n are in good agreement with those obtained by these authors.

The TKE budgets of the ABL and SBL for $\mu = 0$ and various values of C_1 are presented in Figs. 6 and 7. From these figures, the shear production term $N_i^n(z_i^n) = [(\eta_i^n)^2 + (\sigma_i^n)^2](K_i^n)^{-1}$ and the dissipation term $D_i^n(z_i^n) = (E_i^n)^2(K_i^n)^{-1}$ are shown to play a major role in the budget of TKE. The notable feature is that the diffusion term F_i^n also has an important role in the TKE budget in the lower/upper parts of atmosphere/sea. The diffusion of TKE in ABL obtained from models of ASI in which the diffusive flux is not considered is similar to the diffusion of ABL over land at $\mu < 0$; in the lower part of ABL, the diffusive flux coincides in sign with the TKE production terms, and it has opposite sign and less magnitude in the case of $\mu > 0$. From the graphs of TKE budget, it is clear that F_1^n and F_2^n change sign (at $C_1 = 1$) in certain parts, and they coincide with F_1^n and F_2^n at $C_1 = 0$ at certain heights/depths. We can see that the wave layer has much more effect on diffusion than on the shear production and dissipation terms. The results presented in these figures are ob-

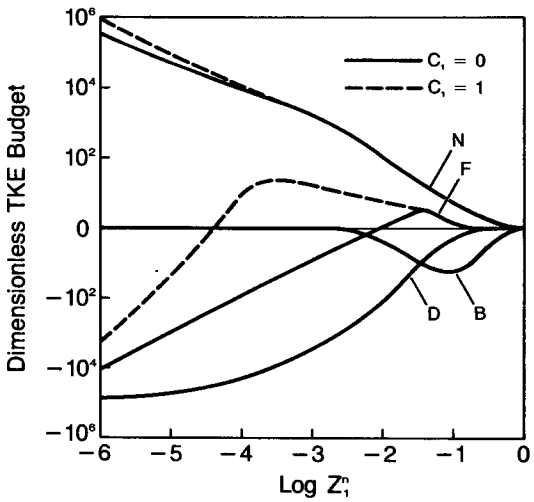

FIG. 6. Dimensionless TKE budget for the atmosphere showing shear production, N, dissipation, D, buoyant production, B, and diffusion, F, at neutral condition ($\mu = 0$) with $C_1 = 0$ and $C_1 = 1$.

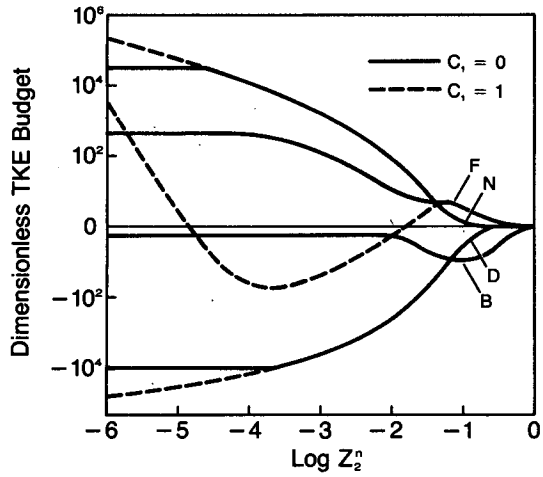

FIG. 7. As in Fig. 6 but for the sea.

tained for the cases $C_1 = 0$ and $C_1 = 1$. However, waves have much more effect on the TKE budget if $C_1 = 10$.

It is worth noting that the large changes in magnitude and in sign happen only with diffusion of TKE. This shows that diffusion of TKE in the ABL and SBL acts as a regulator of TKE, not only in each BL, but also in the whole air–sea system. The model results of the TKE budget and interpretation of the wave layer qualitatively agree with observations of the effect of waves by Kitaigorodski (1970), Lai and Shemdim (1971), and Benilov et al. (1978), and with the modeling results of TKE budget of Klein and Coantic (1981).

To demonstrate the modeling results of the TKE budget, I compare the model results with the experimental estimation of Dubov et al. (1974), who used observational data from the North Atlantic Ocean and the Baltic Sea (for neutral conditions and wind velocity 3–10 m s^{-1} at a height of 5 m over sea surface) to estimate magnitudes of shear production N and dissipation D. The comparison shows good agreement in Figs. 8 and 9.

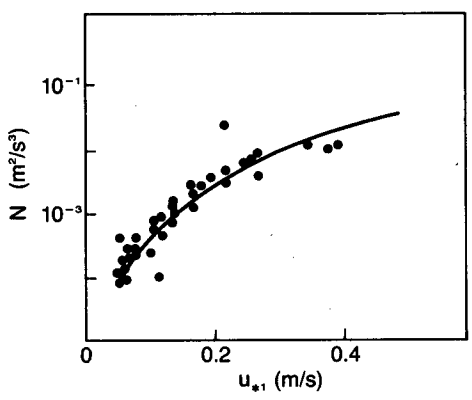

FIG. 8. Shear production, N, as a function of friction velocity u_{*1} at $\mu = 0$ and $z_1 = 5$ m in comparison with estimates by Dubov et al. (1974). The solid curve is our theoretical computation.

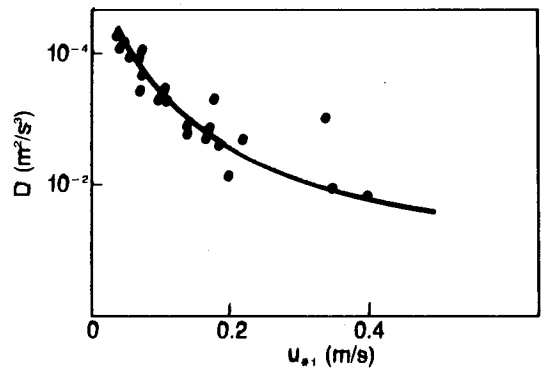

FIG. 9. Dissipation, D, as a function of friction velocity u_{*1}. Symbols are as in Fig. 8.

It is noted that an estimation of the TKE budget over the sea is complicated by the necessity of calculating the wave influence on the air flow. Due to the influence of waves on the lower part of ABL, the wave-induced fluctuations are present (see Lai and Shemdim, 1971; Dubov et al., 1974). This creates a surface wave-induced component in the TKE budget. Hence, it is necessary to take into account the local dissipation of wave-induced fluctuation of wind velocity, variation of TKE with height and additional momentum flux (see Dubov et al., 1974). There is no method of calculating these additional terms precisely, but rather, they are estimated from observational data.

Figures 10 and 11 show the vertical profiles of the

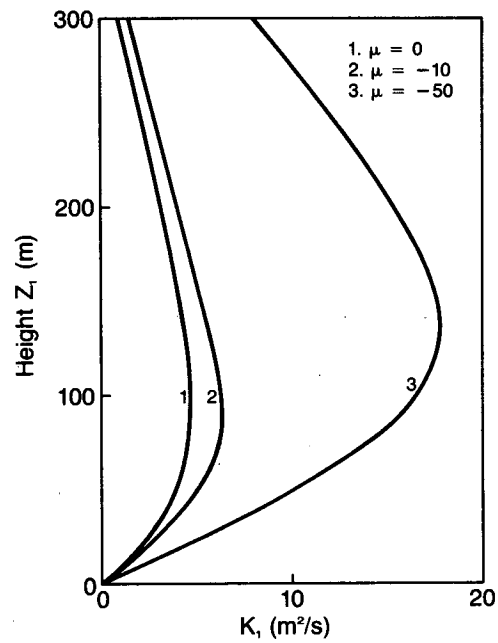

FIG. 10. Vertical profiles of TEC (K_1) for the atmosphere at $U_{g1} = 10$ m s^{-1}, $C_1 = 0$ and $\mu = 0, -10, -50$.

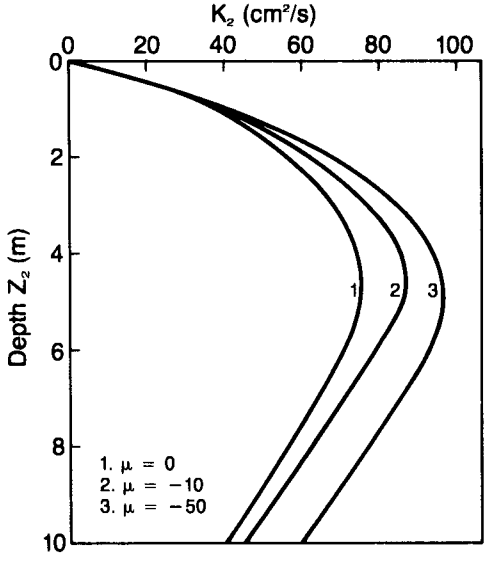

FIG. 11. As in Fig. 10 but for the sea.

dimensional TEC at $U_{g1} = 10$ m s^{-1}, for $\mu = 0, -10, -50$ and $C_1 = 0$ in the ABL and SBL. As we can see from Figs. 10 and 11, the eddy coefficients applicable to the atmosphere and sea increase with increasing U_{g1} and atmospheric instability. The TEC in the sea, K_2 weakly depends on the stability of the atmosphere (K_2 increases with increasing instability in atmosphere), reaches a maximum at a depth of 5 to 7 m, and then decreases smoothly to zero depth. The model results of TEC in the atmosphere and sea agree with the general understanding about the TEC.

Figures 12–15 show the variations of the geostrophic coefficient χ, the angle between surface shear stress and geostrophic wind α_1, the surface drift current velocity U_{02}, and the 10-m height wind velocity U_{10}, and their dependence on U_{g1} for various μ and C_1. It is obvious

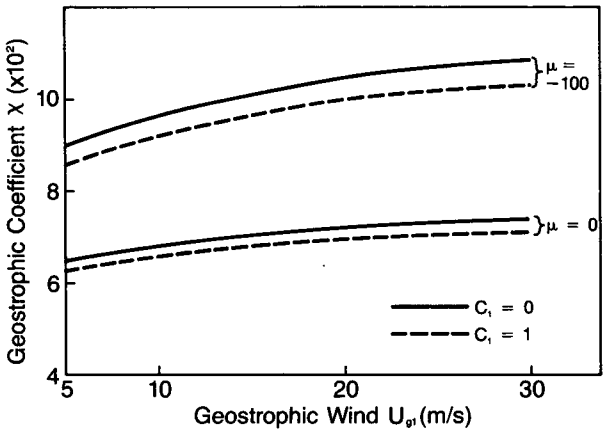

FIG. 12. Geostrophic coefficient, χ, as a function of geostrophic wind U_{g1} at various μ and C_1.

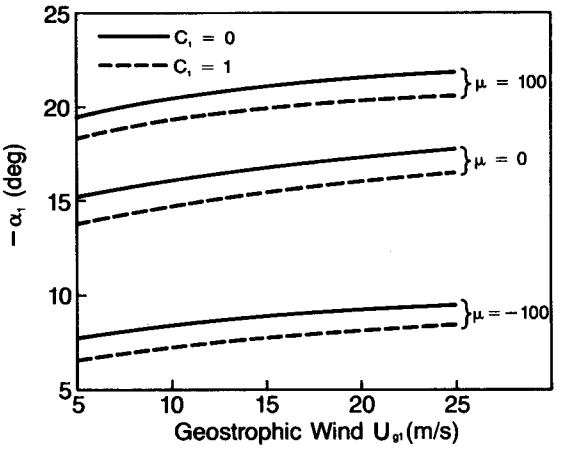

FIG. 13. Dependence of the angle, α_1, between U_{g1} and the surface shear stress on U_{g1} at various μ and C_1.

from these figures and also Table 1 that the influence of waves appears in almost all characteristics of the ASI and depends on μ. These influences are most evident for unstable conditions of the atmosphere and much less notable for stable conditions, i.e., the U_{02} and U_{10} dependence on C_1 is much less for $\mu = 0$ and $\mu = +100$ than for $\mu = -100$.

Figure 12 shows that the geostrophic coefficient χ, strongly depends on C_1 (decreases with increasing C_1) and stability of the atmosphere μ. The angle between surface shear stress and geostrophic wind ($-\alpha_1$) increases with U_{g1} and decreases with growing instability of the atmosphere and C_1 (Fig. 13). The reduction of ($-\alpha_1$) may be connected with an increase of momentum exchange in the ABL, and also, a large increase

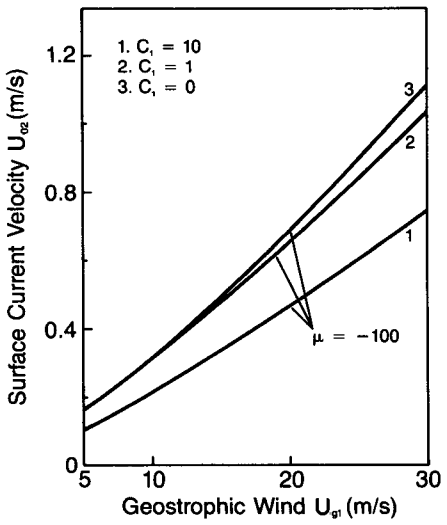

FIG. 14. Dependence of the surface drift current velocity U_{02} on U_{g1} at different C_1 for $\mu = -100$.

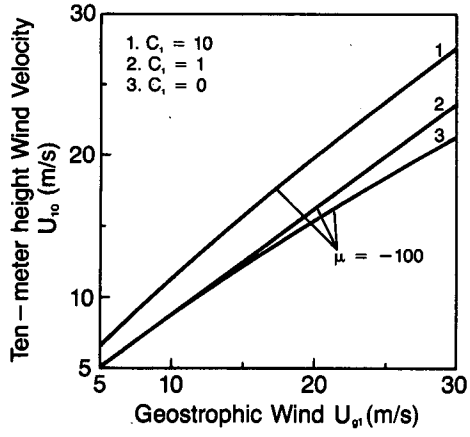

FIG. 15. Dependence of 10-m height wind velocity U_{10} on U_{g1} at various C_1 and $\mu = -100$.

of $(-\alpha_1)$ with increasing stability of the atmosphere is likely a result of decoupling between adjacent layers.

The surface drift velocity, U_{02}, increases with increasing instability in the atmosphere and stability in sea (compare $\mu = 0$ values from Table 1 with $\mu = -100$ values from Fig. 14), i.e., with increasing momentum exchange between the upper and lower parts of ABL. From Fig. 14, we can see that U_{02} decreases with increasing C_1. Physically, this is interpreted to mean that, at $C_1 \neq 0$, a part of the energy transferred to the surface water by wind goes into wave generation; i.e., in this case, not all the energy transferred from the wind goes toward generation of drift current (e.g., Phillips, 1977). This can be seen from the following analysis of (1) and (3). We multiply the first equation of (1) by u and the second by v and add them together with (3) to get the following:

$$\frac{d}{dz}K\frac{d}{dz}\left(\frac{u^2+v^2}{2}\right) - C\frac{E^2}{K} + \alpha_e\frac{d}{dz}K\frac{dE}{dz} = 0. \quad (51)$$

Integrating z from z_0 to $+\infty$, we have

$$-K\frac{d}{dz}\left(\frac{u^2+v^2}{2}\right)\Big|_{z_0} - C\int_{z_0}^{+\infty}\frac{E^2}{K}\,dz - \alpha_e K\frac{dE}{dz}\Big|_{z_0} = 0. \quad (52)$$

From (52) we can see that, if the wave layer is absent [i.e., the diffusion equals zero at the sea surface $\alpha_e K(dE/dz) = 0$ at z_0], all the energy transferred from the wind goes toward generation of a drift current, U_{02} [represented by the first term on the left-hand side of (52)]. If diffusion is not zero at z_0, a part of the energy transferred from the wind goes into wind wave generation, and hence less to the drift current.

Figure 15 shows how the wind velocity at the 10-m height, U_{10}, depends on U_{g1} for various C_1. We can see that U_{10} increases with growing C_1. This evidently results from the presence of the wave layer when the lower part of ABL is strongly turbulent; i.e., in this part of atmosphere, the "pseudoturbulence" acts strongly. Here not only the random turbulent fluctuations of wind velocity exist, but also a wave-stimulated pseudoturbulent fluctuation of various scales (see Stewart, 1968; Benilov et al. 1978). The additional Reynolds fluxes $\overline{u'_a u'_w}$, $\overline{w'_a w'_w}$, $\overline{u'_a w'_w}$, $\overline{u'_a w'_w}$, etc., may be present, where (u'_a, v'_a, w'_a) and (u'_w, v'_w, w'_w) are components of the turbulent fluctuation of wind velocity and of fluctuation due to wave-induced motions, respectively. For this reason the turbulences in the lower/upper parts of the air/sea are increased. Consequently, the wind velocity in the lower part of atmosphere is increased.

Figures 16–19 show comparisons of the model results for the drag coefficient, C_D, the friction velocity, u_{*1}, and the roughness parameter (hereinafter the parameter z_{01} is identified as z_0) z_0, with published results.

The C_D observed over a natural water surface has been studied by many investigators. Most of the observed C_D measurements reported in the literature are associated with near neutral stability stratification $\mu \approx 0$ (see Geernaert et al., 1986; Geernaert and Katsaros, 1986). The theoretical computations of drag coefficient C_D and corresponding observational data at various values of C_1 and $\mu = 0$ are present in Figs. 16 and 17. Figures 16 and 17 were taken from the work of Geernaert et al. (1986). The value of C_D was computed by (42) and is plotted along with observational data obtained by various investigators after Geernaert et al. (1986). From Fig. 16, we can see the strong dependence of C_D on the wave effect, which was noted by Deleonibus (1971) and Geernaert et al. (1986). It is noted from Table 1 and Fig. 16 that $C_1 = 0$ gives larger values of C_D in comparison with $C_1 = 1$, which match better the observational data (see Fig. 16). Therefore, the air–sea interaction models without an explicit wave

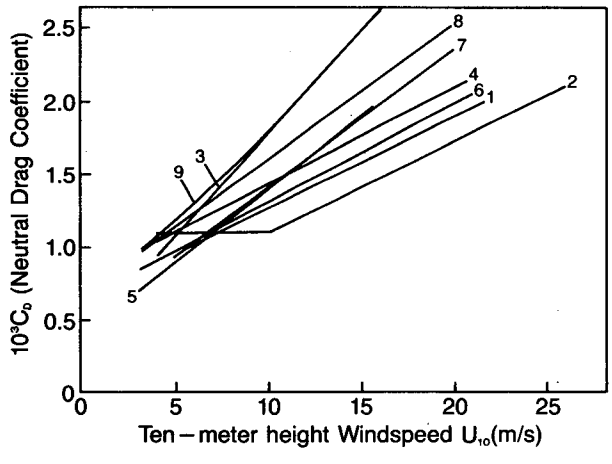

FIG. 16. Published drag coefficient, C_D, as a function of 10-m height windspeed (U_{10}): 1) Smith, 1980; 2) Large and Pond, 1981; 3) Donelan, 1982; 4) Garratt, 1977; 5) Sheppard, 1972; 6) Smith and Banke, 1975; 7) Geerhaert et al. 1986; 8) this model at $C_1 = 1$; 9) this model at $C_1 = 0$. (After Geernaert et al., 1986.)

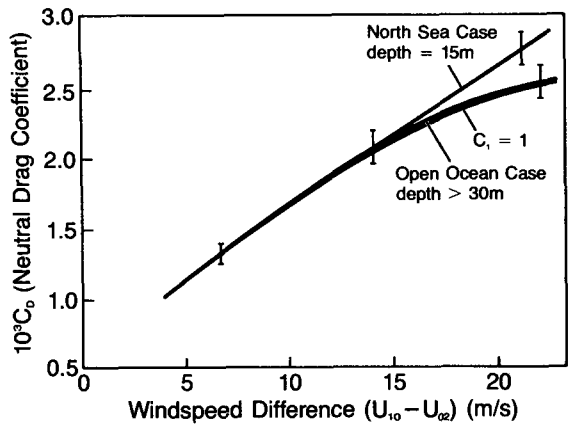

FIG. 17. Values of the drag coefficient, C_D, as a function of windspeed difference for the case of a 15-m water depth, for deep water and for this model at $C_1 = 1$. (After Geernaert et al., 1986.)

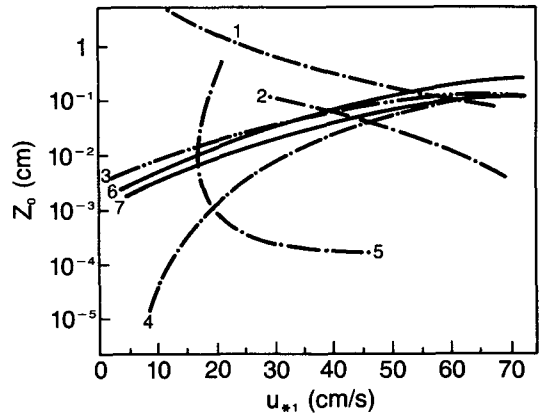

FIG. 19. Roughness parameter, z_0, as a function of friction velocity, u_{*1}, according to: 1) Francis, 1953; 2) Goptarev, 1957; 3) Neumann, 1956; 4) Kuznetsov, 1963; 5) Deacon and Webb, 1962; 6) this model at $C_1 = 0$; 7) this model at $C_1 = 1$. (After Kitaigorodski, 1970.)

layer seem to give larger values of the drag coefficient than are derived from observational data. The theoretical computations of C_D are in good agreement with observational data in Fig. 16, and the trend suggests that larger values of C_1 would match observations even better. The largest discrepancy between measured results occurs, probably, because the observations occur in different atmospheric and sea states. As shown in Fig. 17, C_D is in excellent agreement with the deep-sea results.

In Figs. 18 and 19, the computational friction velocity u_{*1} as a function of wind speed U_{10} for neutral stability ($\mu = 0$) and the computed roughness parameter

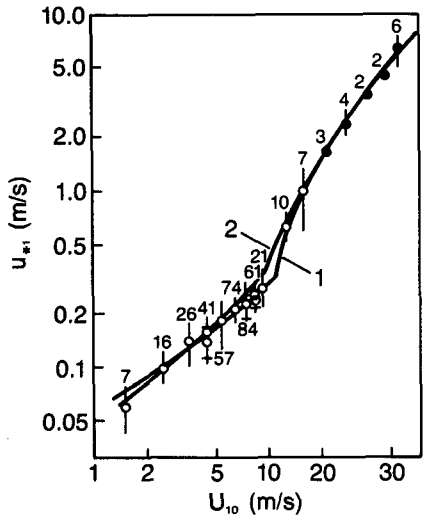

FIG. 18. Friction velocity, u_{*1}, as a function of the 10-m height wind speed U_{10}. Figures near the circles indicate the sample size. The vertical lines give the standard deviations from the mean value u_{*1}. Two dots are given for large samples. Standard deviations corresponding to the latter case are marked by horizontal marks on the vertical lines: 1) Myers, 1959; Kuznetsov, 1970; 2) this model at $C_1 = 0$. (After Kitaigorodski, 1970.)

z_0 as a function of u_{*1} at $\mu = 0$ and various C_1 have been plotted, along with the results of different investigators as shown by Kitaigorodski (1970). The model results are in excellent agreement with observational u_{*1} obtained by Kuznetsov (1970) and Myers (1959) (after Kitaigorodski, 1970) in Fig. 18 and with observational z_0 obtained by various investigators as shown in Fig. 19.

7. Conclusions

In the present model, the wave layer, which is characterized by a discontinuity of velocity, TKE and wind energy transferred across the interface, is taken into account by a parameterization technique. By varying influence of waves through the parameter C_1, we can study numerically the influence of waves of various intensities on the structure of the ABL and SBL.

The results of the simulations show that the wave layer influences almost all characteristics of both the atmosphere and sea, and that TKE generation in the sea surface layer is related, not only to shear production, but also to the TKE diffusive flux. Diffusion has an important effect in the TKE budget, at least in the zones of the atmosphere and sea close to the interface, and acts as a TKE regulator, not only in each boundary layer, but in the whole air–sea system.

The computational results confirmed that the wave layer plays a role of additional source of TKE for the lower/upper parts of ABL/SBL, and that the TKE in these zones very strongly depends on the wave effect and is almost independent of stability.

The model results show that when the wave layer is present the surface drift velocity decreases its magnitude with increasing C_1 because a part of the energy transferred to the surface water by wind goes into wave generation; i.e., not all the energy from wind goes into drift current generation. The wind velocity at the 10-

m height increases with increasing C_1, probably because of the existence of random turbulent fluctuations of the wind velocity and wave-stimulated pseudoturbulent fluctuation of various scales. The drag coefficient strongly depends on C_1 and stability.

The theoretical computations agree well with observational data and the generally accepted understanding about the wave layer.

Acknowledgments. The author expresses his appreciation to Dr. Eugene S. Takle for help, encouragement, editing and the opportunity to return to the field. He is grateful to the Department of Agronomy of Iowa State University for financial support in writing and completing this work. This research was supported, in part, by the Division of Atmospheric Science, National Science Foundation, under Grant ATM-8217210. The author thanks Dr. Gerald Geernaert for his interest, careful reading of the early manuscript and very helpful suggestions and also for use of his two graphs. Thanks are also given to Ms. Linda Claussen for the typing.

REFERENCES

Benilov, A. Yu, A. I. Gumbatov, M. M. Zaslavski and S. A. Kitaigorodski, 1978: A nonstationary model of development of the turbulent boundary layer over the sea with generation of surface waves. *Izv. Acad. Sci. USSR, Atmos. Oceanic Phys.*, **11**, 830–836.

Blackadar, A. K., 1962: The vertical distribution of wind and turbulent exchange in a neutral atmosphere. *J. Geophys. Res.*, **67**, 3095–3102.

Charnock, H., 1955: Wind stress on a water surface. *Quart. J. Roy. Meter. Soc.*, **81**, 639–640.

Deacon, E. L., and E. K. Webb, 1962: Interchange of properties between sea and air; small-scale interaction. *The Sea*, Vol. 1, M. N. Hill, Ed., Wiley-Interscience, 43–87.

Deardorff, J. W., 1972: Numerical investigation of neutral and unstable planetary boundary layer. *J. Atmos. Sci.*, **1**, 91–115.

Deleonibus, P. S., 1971: Momentum flux and wave spectra observations from an ocean tower. *J. Geophys. Res.*, **27**, 6506–6527.

Donelan, M. A., 1982: The dependence of the aerodynamic drag coefficient on wave parameters. Preprints *First Int. Conf. on Meteorology and Air–Sea Interaction of the Coastal Zone.* The Hague, Amer. Meteor. Soc., 381–387.

Dubov, A. S., Ed., 1974: *Processes of Transfer near the Surface of the Ocean—Atmosphere Interaction.* Hydromet. Publishing House, 239 pp.

Egorov, K. L., 1984: An estimate of wave influence on the dynamic structure of the flow over the water. *Izv. Acad. Sci., USSR, Atmos. Oceanic Phys.*, **12**, 1183–1188.

Elder, F. C., D. L. Harris and A. Taylor, 1970: Some evidence of organized flow over natural waves. *Bound.-Layer Meteor.*, **1**, 80–87.

Francis, J. R. D., 1953: A note on the velocity distribution and bottom stress on a wind-driven water current system. *J. Mar. Res.*, **12**, 93–98.

Garratt, J. R., 1977: Review of drag coefficient over oceans and continents. *Mon. Wea. Rev.*, **105**, 915–929.

Geernaert, G., and K. Katsaros, 1986: On the general derivation of the neutral drag coefficient. *J. Phys. Oceanogr.* (in press).

——, —— and K. Richter, 1986: Variation of the drag coefficient and its dependence on sea state. *J. Geophys. Res.* (in press).

Kalatski, V. I., 1969: Influence of parameters of the transitional layer in air–sea interaction. *Trans. Hydrometeor. Center*, **51**.

Kazanski, A. B., and A. C. Monin, 1960: On the turbulent conditions higher atmospheric surface layer. *Izv. Acad. Sci., USSR, Atmos. Oceanic Phys.*, **1**, 165–168.

Kitaigorodski, S. A., 1970: *The Physics of Air–Sea Interaction,* Hydromet. Publishing House, 284 pp. [Transl., Israel Program for Scientific Translations, 1973.]

——, and Yu. A. Bolkov, 1965: On the computation of heat and moisture fluxes in the atmospheric surface layer. *Izv. Acad. Sci., USSR, Atmos. Oceanic Phys.*, **12**, 1319–1336.

——, and Yu. Z. Miropolski, 1969: Estimates of the turbulence in the wind-mixed layer of the ocean. *Okeanology*, **1**, 33–34.

Klein, P., and M. Coantic, 1981: A numerical study of turbulent processes in the marine upper layers. *J. Phys. Oceanogr.*, **11**, 849–863.

Kuznetsov, O. A., 1970: Results of an experimental investigation of the airflow over the sea surface. *Izv. Acad. Sci., USSR, Atmos. Oceanic Phys.*, **8**, 798–803.

Lai, R. J., and O. H. Shemdim, 1971: Laboratory investigation of air turbulent above simple water waves. *J. Geophys. Res.*, **30**, 7334–7350.

Laikhtman, D. L., 1961: *The Physics of the Atmospheric Boundary Layer.* 1st ed., Hydromet. Publishing House, 200 pp. [Transl. Israel Program for Scientific Translations, 1964.]

——, 1966: The dynamics of the boundary layers of the atmosphere and the sea with interaction and nonlinear effects taken into account. *Izv. Acad. Sci., USSR, Atmos. Oceanic Phys.*, **10**, 1017–1025.

——, 1970: *The Physics of the Atmospheric Boundary Layer,* 2nd ed., Hydromet. Publishing House, 340 pp.

——, 1979: On the structure of the atmospheric surface layer. *Izv. Acad. Sci., USSR, Atmos. Oceanic Phys.*, **15**, 682–684.

Large, W. G., and S. Pond, 1981: Open ocean momentum flux measurements in moderate to strong winds. *J. Phys. Oceanogr.*, **11**, 324–336.

Ly, Le N., 1981: On the parameterization of the oceanic atmospheric boundary layers. *Z. Meteor.*, **31**, 367–369.

——, 1984: Interaction between atmospheric and oceanic baroclinic boundary layers. *Z. Meteor.*, **34**, 75–81.

Mellor, G. L., and P. A. Durbin, 1975: The structure and dynamics of the ocean surface mixed layer. *J. Phys. Oceanogr.*, **5**, 718–728.

Monin, A. S., and A. M. Obukhov, 1954: The basic regularities of turbulence in the atmospheric surface layer. *Trans. Geophys. Inst. Akad. Nauk.*, **24**(51), 163–187.

——, and Yaglom, 1965: *Statistical Fluid Mechanics, Mechanics of Turbulence.* Nauka Publishing House, 639 pp.

Myers, V. A., 1959: Surface friction in a hurricane. *Mon. Wea. Rev.*, **8**, 307–311.

Neumann, G., 1956: Wind stress on water surfaces. *Bull. Amer. Meteor. Soc.*, **5**, 211–217.

Phillips, O. M., 1977: *The Dynamics of the Upper Ocean,* 2nd ed., Cambridge University Press, 336 pp.

Roll, H. U., 1965: *Physics of the Marine Atmosphere,* Academic Press, 426 pp.

Sheppard, P. A., D. T. Tribble and J. R. Garratt, 1972: Studies of turbulence in the surface layer over water (Lough Neagh). Part I: Instrumentation, programme, and profiles. *Quart. J. Roy. Meteor. Soc.*, **98**, 627–641.

Smith, S. D., 1980: Wind stress and heat flux over the ocean in gale force winds. *J. Phys. Oceanogr.*, **10**, 709–726.

——, and E. G. Banke, 1975: Variation of the sea surface drag coefficient with wind speed. *Quart. J. Roy. Meteor. Soc.*, **101**, 665–673.

Stewart, R. W., 1968: Small scale interaction between atmosphere and ocean. *The Main Problems of Oceanology.*, Nauka Publishing House, 20–29.

Takle, E. S., R. L. Sani and L. P. Chang, 1982: A diabatic, turbulent, atmospheric boundary layer model. *Finite Element in Fluids*, R. H. Gallagher, D. H. Norrie, J. T. Oden and O. C. Zienkiewicz, Eds., Wiley & Sons, 347–363.

Tarnopolski, A. G., and V. A. Shnaydman, 1984: Modeling the interacting atmospheric and oceanic boundary layers. *Meteor. Hydrol.*, **5**, 48–56.

Wyngaard, J. C., 1975: Modeling the planetary boundary layer—extension to the stable case. *Bound.-Layer Meteor.*, **9**, 441–460.

Yeh, G.-T., 1973: The effect of thermal stratification and evaporation on geostrophic drag coefficient in the atmospheric boundary layer. *Mon. Wea. Rev.*, **101**, 617–623.

——, 1974: Interaction between the atmospheric and oceanic boundary layers. *Bound.-Layer Meteor.*, **1**, 21–37.

Zilitinkevich, S. S., 1970: *Dynamics of the Atmospheric Boundary Layers*. Hydromet. Publishing House, 290 pp.

——, and D. L. Laikhtman, 1965: Turbulent conditions in the near-surface layer of atmosphere. *Izv. Acad. Sci., USSR, Atmos. Oceanic Phys.*, **2**, 150–156.